Rotorcraft thickness noise control

O. SZULC

*Institute of Fluid-Flow Machinery, Polish Academy of Sciences, Fiszera 14,
80-231 Gdansk, Poland, e-mail: Oskar.Szulc@imp.gda.pl.*

THE PAPER DESCRIBES AN INNOVATIVE IDEA OF THICKNESS NOISE CONTROL (TNC) based on adoption of a flow control strategy (i.e. surface ventilation) for acoustic attenuation of helicopter rotor periodic noise. The TNC method is relying on incorporation of multiple cavities (closed by perforated panels and linked to low- and high-pressure reservoirs) located in a symmetrical manner at front and rear portions of the blade tip. The efficiency of the new approach is verified using a two-bladed model rotor of Purcell (untwisted variant of the blade of Bell UH-1H Iroquois helicopter) in low-thrust hover conditions. The results of numerical simulations, obtained with CFD solver (Spalart–Allmaras turbulence and Bohning–Doerffer transpiration models), indicate that in the near-field of the blade tip, both the amplitude and spectral contents of pressure impulses of emitted thickness noise are significantly improved. The TNC method, in the proposed unsteady mode of operation, turns out to be a suitable means of thickness noise reduction in forward flight. Moreover, it is demonstrated that by proper azimuthal activation the efficiency is almost unaltered, while the rotor torque penalty and required transpiration mass-flux are decreased by a factor of 3–5 compared to a steady arrangement.

Key words: helicopter rotor, aerodynamics, aeroacoustics, CFD, noise reduction, active flow and noise control, surface transpiration, perforation.

Notation

Acronyms

ANC	active noise control,
ART	active rotor technology,
AT	active twist,
BD	Bohning–Doerffer,
BVI	blade-vortex interaction,
CFD	computational fluid dynamics,
DFFT	discrete fast Fourier transform,
HHC	higher harmonic control,
HSI	high-speed impulsive,
IBC	individual blade control,
NASA	National Aeronautics and Space Administration,
RANS	Reynolds-averaged Navier–Stokes (equations),
SA	Spalart–Allmaras,

SLIP   symmetric limited positive,
TNC   thickness noise control,
TPP   tip path plane,
URANS   unsteady RANS.

Roman letters

c chord length, m,
c_0 reference (ambient) speed of sound, $\mathrm{m \cdot s^{-1}}$,
c_m blade pitching moment coefficient,
c_q rotor torque coefficient,
c_t rotor thrust coefficient,
f frequency of rotation, Hz,
F_t rotor thrust force, N,
k summation index,
M_q rotor shaft torque, $\mathrm{N \cdot m}$,
M_r Mach number towards the observer,
M_T tip Mach number,
M_θ blade pitching moment, $\mathrm{N \cdot m}$,
n harmonic number,
N sample count,
$OASPL$ overall sound pressure level (dB),
p static pressure, Pa,
p_0 reference (ambient) pressure, Pa,
$\mathrm{p_0}$–$\mathrm{p_4}$ acoustic pressure p' extraction points,
p_aero aerodynamic porosity of the perforated plate,
p_c cavity pressure, Pa,
p' acoustic pressure, Pa,
p'_ref threshold of human hearing, Pa,
p'_rms root mean square of p', Pa,
r distance to the observer, m,
R radius, m,
$\mathrm{Re_T}$ tip Reynolds number,
S surface area, $\mathrm{m^2}$,
SPL sound pressure level (dB),
t time, s,
T period of rotation, s,
T_0 reference (ambient) temperature, K,
V_n normal velocity, $\mathrm{m \cdot s^{-1}}$,
V_t transpiration velocity, $\mathrm{m \cdot s^{-1}}$,
V_T tip velocity, $\mathrm{m \cdot s^{-1}}$,
$x,\, y,\, z$ space coordinates, m,
y^+ non-dimensional distance to the surface.

Greek letters

$\Delta OASPL$ overall sound pressure level reduction (dB),
θ collective angle, °,
μ_0 reference (ambient) viscosity, $\mathrm{Pa \cdot s}$,
ρ_0 reference (ambient) density, $\mathrm{kg \cdot m^{-3}}$,
τ retarded time, s,
ψ azimuthal position angle, °.

1. Introduction

Near the Tip Path Plane (TPP) of a helicopter rotor the recorded acoustic pressure signal has a typical, symmetrical form, with large amplitude negative impulse that is emitted mostly forward of the flying aircraft, frequently becoming a dominating source of rotorcraft noise [1]. From the point of view of civil and military missions noise radiation constitutes a major concern, rising the community annoyance and extending the detection range of approaching helicopters. In case of modern rotor designs, usually operating in forward flight with the advancing tip Mach numbers below 0.8, the shape of the pulse may be explained by the linear acoustic analogy theory. Moreover, it is only sufficient to consider the kinematic thickness (monopole) term of the far-field solution (e.g. Farassat's formulation 1 [2]) of inhomogeneous linear wave equation originally proposed by Lighthill for jet-noise predictions. It was later generalised by Ffowcs Williams and Hawkings [3] to configurations involving arbitrary movement of acoustic source surfaces (e.g. helicopter rotor or propeller blades). At the given observer location in space (x, y, z) the acoustic pressure fluctuation p' [Pa] $= p - p_0$ (p – static pressure, p_0 – reference pressure) at any moment of time t [s] is evaluated as a rate of change of the integral of elementary acoustic sources (monopoles) spread over the whole blade surface S [m^2]:

$$(1.1) \qquad 4\pi\, p'(x, y, z, t) = \frac{\partial}{\partial t} \int\limits_{S} \left[\frac{\rho_0 V_{\mathrm{n}}}{r|1 - M_r|} \right]_{\mathrm{ret}} dS.$$

The integrated potential of a single discrete acoustic source panel dS [m^2] is calculated at the emission time τ [s] $= t - r/c_0$ (retarded time formulation, c_0 [m $\cdot$ s^{-1}] – constant speed of sound), and depends on four physical parameters: ρ_0 [kg $\cdot$ m^{-3}] – constant ambient density, V_{n} [m $\cdot$ s^{-1}] – projection of panel velocity vector due to rotation on the surface normal direction, r [m] – distance from the panel centre to the observer location, and M_{r} – Mach number based on the projection of panel velocity vector due to rotation on the direction towards the observer. As may be deduced from Eq. (1.1), the monopole radiation is a consequence of the blade surface shape and movement alone, independent of the external air-flow (exerted forces). As a result of modelling a nearly symmetrical acoustic pulse is predicted, similar to the reference signal of Fig. 3 (marked as "TNC off"). It is necessary to notice that in the TPP of contemporary helicopter rotor designs, operating in subsonic conditions regardless of hover or the forward flight state, the generated harmonic noise pattern is dominated by the thickness component, but still a small contribution related to the in-plane force is present as well.

There are many sources of noise associated with a flying helicopter, e.g.: engine, transmission, airframe, and both rotors [4, 5]. However, the majority of the

current research in the field is focused on the main and tail rotors operation, since these two components alone are responsible for most of the acoustic radiation in flight. The tail rotor plays an important role for observers positioned relatively close to the helicopter, where its higher frequency noise has not yet been attenuated by the atmosphere. Additionally, it may become particularly annoying due to its higher frequency (compared to the main rotor), placed directly in the range in which the human hearing is most sensitive. Nevertheless, the distinctive acoustic emission of the tail rotor has rather low impact on the aural detection range of an approaching helicopter, therefore it is not considered in the paper. On the other hand, during approach the noise from the main rotor completely dominates the acoustic signature of a helicopter. Due to its large amplitude, low-frequency spectral contents, and strong forward directivity pattern, the main rotor noise is weakly attenuated and propagates for great distances in the atmosphere.

Deterministic origins of the main rotor discrete frequency (tonal) noise may be subdivided into several categories. The aforementioned thickness noise (of monopole character) depends on the shape and motion of the blades only, and is emitted primarily in the rotor plane due to the displacement effect of air by the rotating body (equivalent to surface mass transfer). In general, the aerodynamic loading noise (of dipole nature) is affected by steady and unsteady forces exerted by the rotating object on the surrounding fluid elements (equivalent to transfer of momentum). It is directed mainly below the rotor disc. The rotor thickness and non-impulsive loading contributors to acoustic radiation (named rotational noise) are present in all flight conditions, even in hover. A rapid change of pressure distribution forced by close proximity or collision of tip vortices with successive blades is one type of the extreme loading noise called blade-vortex interaction (BVI). In flight it develops either on the advancing or on the retreating side, with the directivity concentrated down and forward or down and rearward respectively. Typically this highly impulsive source occurs in low-speed descent or during maneuvers, but sometimes even in high-speed forward flight. In contrast to thickness, loading noise spectra may exhibit not only harmonic (i.e. local maxima present near the blade passing frequency and its higher multiples), but also broadband character. The stochastic (non-deterministic) nature is attributed to turbulence ingestion, blade-wake interaction, or blade self-noise phenomena. Lastly, in high-speed flyover the advancing blade is subjected to strong compressibility effects (formation of transonic regions and shocks). A periodic formation and decay of normal shock wave is a major volumetric source (quadrupole type) of acoustic perturbations called the high-speed impulsive (HSI) noise. It is especially intense when the shock wave is delocalized off-the tip – a consequence of exceeding the critical advancing tip Mach number (usually above 0.9). Its in-plane and forward directivity pattern is similar to thickness noise, but with

increased amplitude and richer spectral contents, causing much higher annoyance when it appears.

It is known that lowering the hover tip Mach number is an effective means of reducing the helicopter main rotor noise emission (e.g. [6]). This way not only the deterministic (tonal), but also the non-deterministic (broadband) sources are significantly attenuated. The price is often increased operational weight of a helicopter (due to necessary enlargement of the blade surface area and the transmission system). On the other hand, from the safety point of view, the lower tip velocity requires addition of mass to ensure proper autorotation envelope, which further increases the weight of the aircraft. It is also agreed that improvements in the rotor aerodynamic performance by application of non-rectangular blade tip shapes (e.g. thinned, tapered, and swept) are usually accompanied by reductions of acoustic radiation in flight, limiting both the rotational (thickness and non-impulsive loading) and the impulsive (HSI and BVI) contributions (e.g. [7, 8]). Unfortunately, the thinned or tapered tip sections tend to stall prematurely, at lower angles of attack compared to their thicker or untapered counterparts. This introduces undesirable dynamic stall characteristics (i.e. a loss of lift due to massive boundary layer separation), affecting unfavourably the retreating side flow pattern in high-speed forward flight conditions. Moreover, the sweep problem is to avoid significant rearward offset of the aerodynamic centre that may cause adverse aeroelastic effects. Apart from the standard (aerodynamic) sweep, the acoustic sweep concept is developed (patented by NASA) and considered as a feasible remedy to rotorcraft noise [9]. Instead of relying on usual source mitigation, as most of other methods, the proposed non-linear sweep of the rotor blade quarter-chord line provides a smart mechanism of total or partial cancellation of the generated sound waves in the acoustic far-field, regardless of their origin (i.e. monopole, dipole or quadrupole). Another attempt of defocusing the main rotor noise (harmonic) is to increase the number of blades or to apply unequal (modulated) blade spacing [10]. This way, the acoustic spectra are spread more evenly, but on the expense of shifting towards the higher frequency range that rises the subjective annoyance level. However, the higher frequencies are better attenuated by the atmosphere.

Passive methods (i.e. limitation of rotational speed, advanced 3D blade design, and increase of the number of blades), as described above, can be very cost-effective in reduction of various sources of noise attributed to helicopter rotor operations, but still with varying rate of success that is greatly depending on flight conditions and sound radiation directivity. Recently, significant efforts have been focused towards the development of active rotor technologies (ARTs) that have large potential to reduce noise and vibrations, improve performance, and allow adaptation to current flight conditions [1]. Active, on-blade trailing edge

flaps (e.g. using smart materials, such as piezoelectric) provide a viable option to control the acoustic emissions [11]. For example, reduced in-plane, low-frequency noise levels may be achieved by an unsteady flap actuation that augments the in-plane component of blade airloads on the advancing side of the rotor. By this action an additional impulse (of dipole type) is radiated forward that partially offsets the negative pressure peak associated with thickness effects [12]. However, other active rotor technologies rely on the blade root control instead of the on-blade control. The individual blade control (IBC) system is intended to interchange usually rigid pitch links of the rotor pitch control mechanism with servo-hydraulic actuators [13]. These actuators are able to set the pitch of each rotor blade independently of each other. Contrary to IBC, the actuators may be placed below the rotor swashplate as well, introducing the higher harmonic control (HHC) of the blade pitch setting [14]. HHC, while being simpler to design, is also more limited (compared to IBC), because only certain frequencies of excitation may be transferred to the rotating frame, therefore very often noise and vibrations cannot be reduced at the same time. Even more advanced applications of ART are considered that try to integrate actuators into the blade (spar or skin) itself to generate active twist (AT) distributed along the rotor blade radius [15]. In principle, all three mentioned ARTs, i.e.: IBC, HHC, and AT prove to be efficient in BVI noise control, not only by being capable of increasing the blade-tip vortex miss distance, but also unloading the blade in the azimuthal ranges of strong BVI phenomena. They reveal great potential for rotational noise control, allowing for shaping of the pitch schedule of each blade, thus creating an unsteady in-plane force that acts similarly to the periodic deployment of the trailing edge flap. Unfortunately, integration of such advanced active rotor technologies adds a lot of complexity to the rotor system and considerably increases the costs. The active rotors are constantly under research in the United States, the European Union, and Japan, but are not reliable enough to be directly integrated in the current rotorcrafts. No serial production helicopter makes use of quoted active rotor technologies yet.

One possibility to reduce thickness noise emission is to alter physical parameters determining the monopole acoustic potential of Eq. (1.1). It is usually accomplished by modifying the outer shape of the blade (S), utilizing optimised airfoil sections, slanted and thin tips, and decreasing the hover tip Mach number (limiting at the same time V_n and M_r). Assuming the rotational speed of the rotor (M_r) and the blade surface S as fixed, the remaining alternative is to counteract the normal velocity V_n. It could be easily realised by introducing surface mass transfer, i.e. suction and blowing through perforated panels distributed over the blade tip. In theory, such pneumatic systems may be very efficient in thickness noise attenuation, but not without a significant performance penalty. Due to the requested intensity the transpiration affects not only the sound waves

production by a rotating body, but also influences the whole flow-field, i.e. aero-dynamic forces and moments exerted on the blade. Fortunately, it offers an option of deactivation when its operation is not required. However, even though the transpiration is blocked, the perforated surfaces still exhibit increased roughness that may slightly affect the boundary layer development.

It has been experimentally proven lately that a similar in-plane rotor harmonic noise cancelling effect may be achieved by applying a control source of mass and momentum (unsteady tip blowing investigated by Sargent and Schmitz [16]) or a control source of in-plane force (time-dependent trailing edge flap actuation tested i.a. by Shi *et al.* [17]). Both active methods constitute a promising means of rotor thickness noise reduction, but no information regarding the related aerodynamic performance loss is provided. On the other hand, it has already been presented in [18] that for an exemplary model rotor in low-thrust hover conditions the analysed numerically (using CFD) Thickness Noise Control (TNC) method in its steady mode of operation (i.e. constant suction/blowing) is capable of delivering considerable gains in acoustic pressure amplitude reduction (peak amplitude of p' by 46%, overall sound pressure level ($OASPL$) by 3.4 dB, and sound pressure level by 3 dB–10 dB for the lowest 20 rotor harmonics) for an in-plane, near-field observer location. Unfortunately, due to the existence of permanent injection of air the boundary layer is highly disturbed (but not yet separated), leading to a drag increase of the tip sections and rotor shaft torque penalty as large as 38%. Moreover, the steady approach to TNC, being attractive in terms of the directivity pattern (exactly the same efficiency regardless of the azimuthal position of the observer), requires high transpiration mass-flow rates that are rather not feasible for full-scale rotor designs.

In forward flight the maximum of acoustic radiation is centred in the region directly in-front of the helicopter, in a cone approximately of $\pm 15°$ below and above the TPP, and $\pm 15°$ to the left and to the right in relation to the mission path. Therefore, in a such case it is sufficient to concentrate the effort of noise attenuation in the above mentioned zone only, accepting even the eventuality of a slight increase of sound emission everywhere else. The main goal of the paper is to analyse the effect of implementation of the TNC method in unsteady mode of operation which is designed for forward flight conditions (i.e. focused on a single observer, as in [16, 17]). The most important question asked is: is it possible to keep high efficiency of the noise reduction (revealed previously in [18]) with significant limitation of the rotor torque penalty and required transpiration mass-flux? The presented article clarifies this issue, indicating the time-dependant mode as the only one feasible from the point of view of real-world application of TNC. However, the proposed periodic activation/deactivation of fluid injection/extraction process may introduce additional sources of noise on its own. These unsteady side-effects should be resolved by the numerical model

and included in the analysis. Moreover, it is essential to verify, if the introduced short-time disturbances impair the performance of the TNC method in terms of the reduction of the thickness pulse amplitude, or are fairly separated in reception time, not interfering with the main event.

The proposed variant of TNC by perforated wall ventilation may be considered as an extension of the methods described above, since the control source of the anti-noise impulse is not localized, but distributed over a certain portion of the blade surface. It is worth noting that this way the introduced (artificial) sources and sinks of mass may be positioned directly in regions responsible for maximum acoustic radiation in flight, counteracting the main mechanism of thickness noise radiation (source) at its origin. However, the implementation of TNC in the proposed form would necessitate a major re-design of the rotor blades, influencing not only aerodynamic and aeroacoustic properties, but also mass distribution and elastic properties. Such an effort seems to be justified for new blades only. On the other hand, such an optimized rotor could provide significant improvements of the efficiency of the TNC system and reduction of the associated penalties in terms of the aerodynamic performance. The research described in the article fits current efforts of the helicopter industry to limit acoustic waves emission of contemporary rotor designs, for which the main contributor to annoyance and long-range detection is thickness noise.

2. Thickness noise control (TNC) by surface transpiration

The investigated type of the TNC method relies on incorporation of multiple cavities (each linked to compressed gas or vacuum tanks) closed by perforated panels and placed directly at the blade tip (Fig. 1). A pair of relatively short cav-
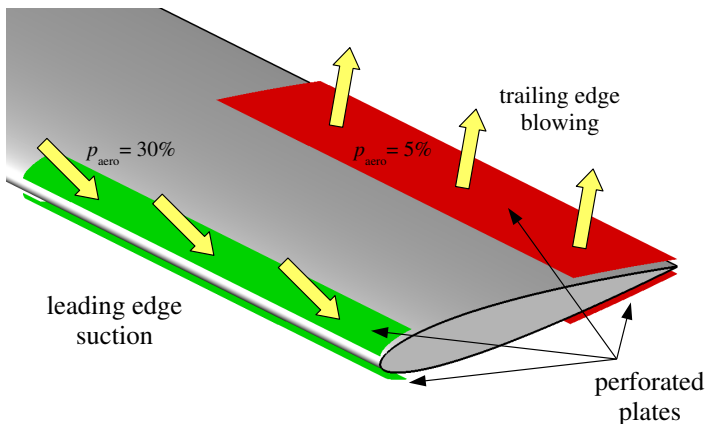

Fig. 1. The tip of a helicopter rotor blade with TNC.

ities, covered by perforated plates of equal (large) porosity p_{aero} and connected to a low pressure supply (resulting in intensive suction of air from the main stream), is positioned in a symmetrical manner (with respect to the chord) near the leading edge (green colour in Fig. 1). In contrast, two remaining identical cavities (built symmetrically into the rear portion of the section) are significantly extended, covered by perforated panels of matching (low) porosity, and connected to a high pressure reservoir (allowing for mild blowing of medium from the plenum) – red colour in Fig. 1. In case of a sufficiently high pressure difference between both sides of the perforation orifice the flow becomes choked. Within the applicable range of porosity values the effective Mach number in each hole is limited to 0.57 [19]. Hence, the resultant transpiration velocity V_t is uniform over the ventilated surfaces, and does not depend on the local flow state. The number, as well as the chordwise/spanwise extent and placement of separate cavities are adapted to locations of maximum values of normal velocity V_n (Eq. 1.1) during blade movement, to suppress the main mechanism of thickness noise radiation. In total the suction and blowing mass-fluxes are not even, but are characterized by 2.4:1 proportionality factor. The excess air could be used to further control the rotor acoustics (e.g. spanwise tip blowing [20]) or just expelled at the root. Until now [18] steady injection and bleed rates have proven to be efficient from the point of view of acoustic attenuation and almost ideal azimuthal directivity pattern, simultaneously leading to an unacceptable aerodynamic performance loss (manifesting itself i.a. as an increase of the rotor shaft torque).

The size and location of the required compressed air/vacuum tanks, the extent of the supply tubes or the energy required to operate the compressor/pump are not considered in the presented investigation of the TNC concept. This theoretical (numerical) study is focused on the impact of TNC on external aerodynamics and aeroacoustics of the isolated rotor only, therefore it is not intended to deliver final details of the actual implementation for a full-scale helicopter. It is worth to emphasize that implementation of a pneumatic system based on perforated panels in external aerodynamics is challenging. One may have to take into account related considerations, such as: the effect of clogging, cleaning requirements, and possible erosion or even damage due to impact of particles (solid and liquid) [21]. These important operational aspects are not covered in the paper either.

In forward flight the acoustic impulses of the largest amplitude are released periodically from the advancing blade, i.e. in an azimuthal section of the rotor disc, exactly when the oscillating inflow Mach number is at maximum. It provides an opportunity of the adaptation of TNC to forward in-plane located observers in order to limit the negative impact of the method on the boundary layer state, and hence on the aerodynamic loading. The single pulse duration time (width) is short (equals to approx. 1.6 ms, equivalent to 20° of azimuth

for the case analysed in Section 5), and corresponds to a certain fraction of the rotation period. Therefore, the TNC system may be activated in a cyclic manner (frequency of 1/rev), just within a limited range of the blade azimuthal position angle ψ (centred at $\psi \approx 90°$). Such an unsteady approach offers a substantial diminution of introduced flow destabilisation and reduction of required intensity of the transpiration compared to steady conditions.

3. Physical and numerical modelling in SPARC solver

This research has been conducted using the SPARC code (formerly named KAPPA) – a standard cell-centred, block-structured, parallel CFD solver developed by Magagnato at the University of Karlsruhe [22]. It solves numerically the Favre-averaged mass, momentum, and energy conservation equations derived for compressible turbulent flow simulations. The effect of turbulent fluctuations is well predicted by a low-Reynolds number eddy-viscosity model of Spalart and Allmaras (SA) for the reference and flow control configurations [23]. The semi-discrete algorithm is based on the 2$^{\text{nd}}$ order finite volume scheme (central approximation of convective and diffusive fluxes) and implicit dual time-stepping approach (supplemented with the Runge–Kutta method) for spatial and temporal discretisations respectively. For stability reasons the SLIP (Symmetric Limited Positive) artificial dissipation model of Jameson is implemented that ensures a proper damping of disturbances in the flow-field. Additionally, the implicit residual smoothing, local time-stepping, and full multigrid strategy improve the convergence rate to a steady state. The equations of motion are formulated in the absolute reference frame, thereby the rotor circulation in space is imposed as a rotation of the entire computational domain. Both, the TNC itself (in the forward flight adapted mode of operation) and the presence of grid movement require the unsteady solution of the problem (unsteady RANS – URANS).

The main capabilities of the SPARC code have been extended by an in-house implementation of the empirical Bohning–Doerffer (BD) transpiration model [19] in a form of the perforated wall boundary condition [24, 25]. In the past, this functionality has been validated against experimental data for basic internal and external flows with surface ventilation [26], and applied in a study of new methods of thickness noise mitigation [18] and high-speed impulsive noise reduction [27]. It is worth noting that the solver has proven its value many times in predictions of complex rotorcraft flows, including helicopter rotors operating in transonic hover and forward flight conditions (e.g. [27–30]). For both configurations, the reference one and equipped with the TNC system, the acoustic post-processing of the CFD results is limited to low-frequency rotor harmonics and near-field observers only. The amplitude damping (dissipation) and shape deformation (dispersion) of the radiated acoustic pressure pulses with increasing

distance from the blade tip is a common feature of the adopted variant of the URANS approach, designed primarily for fast stabilization of rotor loads.

4. Computational model

The efficiency of the TNC method was numerically verified using a $1/7^{\text{th}}$ scale model of the main rotor of the U.S. Army Bell UH-1H Iroquois ("Huey") general utility helicopter, tested experimentally at NASA by Purcell (1988) in low-thrust hover conditions [31]. Both blades of the rotor (diameter of 2.09 m) were straight (untwisted) and rectangular in planform, with the classical NACA 0012 section of the constant chord length c equal to 0.0762 m (the rotor aspect ratio of 13.71). Operating conditions were chosen according to an exploratory experimental study of an equivalent rotor system of Sargent and Schmitz (2012) in the University of Maryland Acoustic Chamber at a full-scale tip Mach number of $M_{\text{T}} = 0.661$ (tip Reynolds number of $\text{Re}_{\text{T}} = 1.6 \cdot 10^6$) and low collective angle of $\theta = 1.5°$ [16]. This research was focused on the efficiency of a recently developed active control method of acoustic cancellation (tip jet blowing), intended for helicopter rotor in-plane harmonic noise reduction. Detailed data regarding the rotor dimensions and operating conditions is summarized in Table 1.

Table 1. Rotor dimensions and operating conditions.

Parameter	$1/7^{\text{th}}$ scale model	CFD model
rotor radius, R [m]	1.045	13.71
blade chord length, c [m]	0.0762	1.0
rotor aspect ratio (R/c)	13.71	13.71
blade collective angle, θ [°]	1.5	1.5
ambient pressure, p_0 [Pa]	101325	10293
ambient temperature, T_0 [K]	288.15	288.15
ambient density, ρ_0 [kg $\cdot$ m^{-3}]	1.225	0.125
ambient viscosity, μ_0 [Pa $\cdot$ s]	$1.79 \cdot 10^{-5}$	$1.79 \cdot 10^{-5}$
ambient speed of sound, c_0 [m $\cdot$ s^{-1}]	340.3	340.3
tip Mach number, M_{T}	0.661	0.661
tip Reynolds number, Re_{T}	$1.6 \cdot 10^6$	$1.6 \cdot 10^6$
tip velocity, V_{T} [m $\cdot$ s^{-1}]	224.9	224.9
frequency of rotation, f [Hz]	34.26	2.61
period of rotation, T [ms]	29.2	383.0
rotational speed [rpm]	2055	157

The computational set-up applied in the current investigation has been extensively validated in the past for Caradonna and Tung model helicopter rotor in transonic hover [27–30], therefore the description of structured grid topology and density, initial and boundary conditions, convergence criteria, and time-step

or mesh dependency studies are not presented here in details. Certainly, some differences are introduced during numerical verification of the TNC method. For example, the blade aspect ratio is up-scaled to 13.71, the collective angle is reduced to 1.5°, operating Mach and Reynolds numbers are fixed to 0.661 and $1.6 \cdot 10^6$, respectively. The near-wall grid normal spacing is adapted to a lower tip Reynolds number of $1.6 \cdot 10^6$, to ensure proper resolution of the boundary layer viscous zone (i.e. $y^+ = \mathcal{O}(1)$). Additionally, an automatic local mesh refinement procedure (increase of the cell count by a factor of 2 in each direction, with non-matching inter-block connections) is performed in all spatial regions taking part in the generation and near-field propagation of the thickness acoustic signal, i.e. 10 blocks enclosing the blade tip and the remaining 14 distributed beyond the tip (radially), near the rotor plane and along the path of the impulse, from the source surface to the chosen observer position (highlighted in red colour in Fig. 2). As a result the number of control volumes of the grid was reduced down to $2.9 \cdot 10^6$ per blade (compared to $7.0 \cdot 10^6$, necessary in transonic flow predictions described in [27, 29]) mainly due to lack of strong compressibility effects, such as shock waves or shock-induced boundary layer separation, in selected fully subsonic conditions. The structured C-H-H grid (80-blocks) topology designed for a single blade is presented in Fig. 2a. The outer boundaries
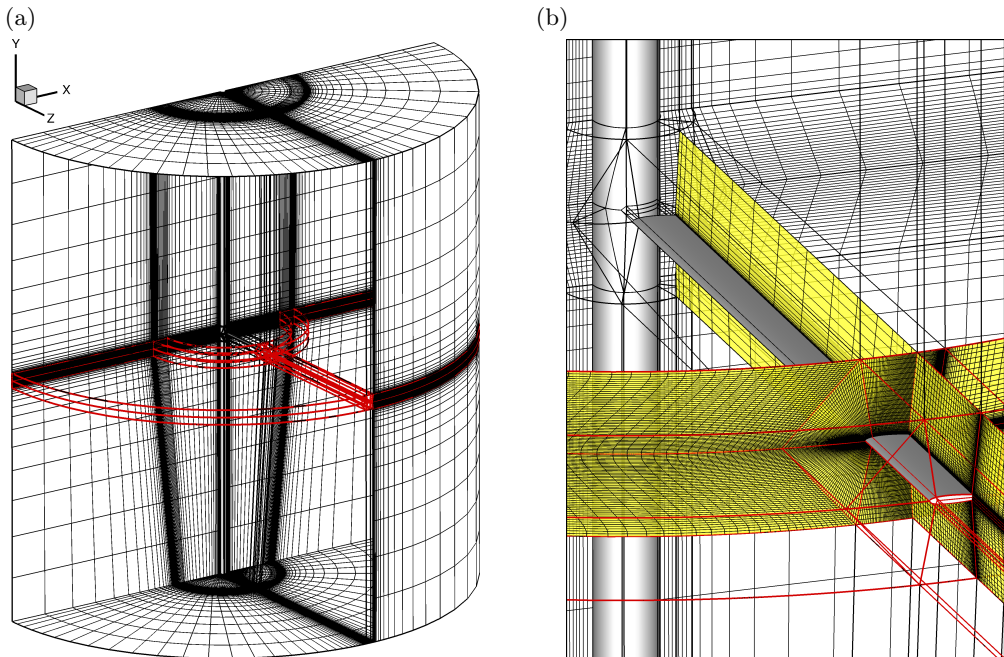

FIG. 2. Purcell rotor multi-block computational grid (80 blocks and $2.9 \cdot 10^6$ control volumes): (a) Complete computational domain. (b) Rotor blade close-up.

of the domain are positioned $3R$ above and below the rotor disc, and $2R$ off the tip, equivalent to $3R$ from the rotation axis (R – rotor radius). The ambient pressure/temperature inlet/outlet boundary condition is utilized there (with automatic back-flow control). The second blade is taken into account by applying the rotational periodicity boundary condition. The rotor blade surface is modelled either with the no-slip (impermeable) wall boundary condition or with the permeable (perforated) wall boundary condition, depending on the case under consideration and face location. Additionally, an artificial hub is implemented in the computational model with the free-slip (impermeable) wall assumption. The yellow colour in a zoomed view of Fig. 2b depicts two exemplary cross-sections (chordwise and spanwise) of the grid near the rotor plane and the blade surface, visualising the basic outline of the volume mesh set-up. Detailed data regarding the rotor computational model is summarized in Table 2.

Table 2. Computational model details.

Domain size	$3R$ from the hub in radial and axial directions
grid type	block-structured (C-H-H) with local grid refinement and non-matching inter-block connections
number of blocks	80 (per blade)
number of volumes	$2.9 \cdot 10^6$ (per blade)
CFD solver	SPARC (finite volume)
flow model	URANS (low-Re Spalart-Allmaras)
transpiration model	Bohning–Doerffer
time step size	$0.25°$ (1440 per period T), equivalent to 0.27 ms
outer surface b.c.	ambient pressure/temperature inlet/outlet
blade surface b.c.	no-slip wall (impermeable or permeable)
hub surface b.c.	slip wall
periodic plane b.c.	rotational periodicity

The theoretical model of the baseline UH-1H helicopter rotor blade was modified by inclusion of two suction and two blowing systems (according to Fig. 1), located at the front (between the leading edge and 0.1c) and at the rear (between 0.65c and the trailing edge) parts of the tip (the last 20% of the span, equivalent to 2.742c), respectively. Two perforated panels of equal, relatively high porosity of 30% covered both forward cavities. In contrast, two perforated panels of equal, low porosity of 5% closed the remaining rearward cavities. The adopted porosities were in line with the range of applicability of the BD model that delivers not only the transpiration flow intensity but also the maximum mass-flow rate achievable in choked conditions. The development of this empirical correlation was based on an experimental study of a set of perforated plates, characterized by porosity values ranging from 2% to 27% [19]. When a sufficiently high pressure difference was imposed to both sides of the orifices, the air in the holes accelerated locally to sonic velocity, choking the flow and fixing the achievable

mass-flow rate of the perforated panel. It has been verified by wind tunnel testing that at such conditions the effective Mach number (corresponding to the measured mass-flow rate) in a single perforation hole was limited to 0.57 (due to existence of boundary layers, inlet effects, shock waves and shock induced separation, etc.). To keep the perforation holes choked the cavity pressure ratio p_c/p_0 was fixed to 0.631 (suction system) and 1.425 (blowing system). The resultant uniform suction ($60\,\mathrm{m\cdot s^{-1}}$) and blowing ($10\,\mathrm{m\cdot s^{-1}}$) rates were a consequence of independence of the transpiration velocity V_t of the local flow conditions present at the ventilated surface. Although in the current arrangement of TNC the surface area subjected to injection of fluid was 3.1 times larger than the surface area intended for bleeding of air, the final mass-flux of suction surpassed the blowing intensity by a factor of 2.4 (i.e. ratio of $2.4:1$). The TNC system parameters and set-up (CFD model) are summarized in Table 3.

Table 3. TNC system set-up (CFD model).

Parameter	Suction system	Blowing system
number of cavities	2	2
number of perforated panels	2	2
chordwise location	$0.0c$–$0.1c$	$0.65c$–$1.0c$
spanwise location	$0.8R$–$1.0R$	$0.8R$–$1.0R$
azimuthal range (steady mode)	$0°$–$360°$ ($360°$)	$0°$–$360°$ ($360°$)
azimuthal range (unsteady mode)	$37.5°$–$112.5°$ ($75°$)	$37.5°$–$112.5°$ ($75°$)
plate porosity (%)	30	5
cavity pressure ratio, p_c/p_0	0.631	1.425
perforation holes	choked	choked
transpiration direction	normal	normal
transpiration velocity, V_t [$\mathrm{m\cdot s^{-1}}$]	60	10
transpiration area [$\mathrm{m^2}$]	0.318	0.991
transpiration mass flux [$\mathrm{kg\cdot s^{-1}}$]	2.74	1.15

What is worth to notice is that even for the TNC method in an unsteady mode of operation, the transpiration intensity is fixed (if present). Instead, during a single rotation period of the rotor blade the holes are intermittently activated and deactivated (almost instantly), depending on the prescribed azimuthal schedule. The activation/deactivation times considered here are equal to a single time step of the numerical scheme (equivalent to $0.25°$ of azimuth). Nevertheless, this approach is referred to as "instantaneous", because the activation/deactivation is undertaken in the shortest possible time allowed by the simulation. This means that there is no pulsating mass-flow rate through orifices and there are practically no increased perforation losses compared to a fully steady mode of operation. Still, due to the aforementioned nature of TNC, the CFD simulation has to be carried out with an unsteady numerical scheme, allowing for

a change in time of the perforated wall properties. Even though the main thickness noise pulse width is short (equivalent to 20° of azimuth for investigated cases), the azimuthal activity range (TNC in unsteady mode) is fixed to 75°, covering approx. $1/5^{\text{th}}$ of the rotor revolution. If the azimuthal activity range is more restricted, not only the width of the anti-noise pulse would be too narrow to have any substantial impact on the generated noise, but also the introduced side-disturbances would grow in amplitude and interfere with the main pulse. Additionally, the in-plane sound radiation directivity pattern would be compromised. The specific design and implementation of the azimuthal activation control system for TNC is not covered in this article. However, regarding the possible mechanisms of 1/rev cyclic control, it seems more beneficial to control the porosity of the plates (hence suction/blowing rates) instead of using traditional pressure valves located at the root of the blade. The main advantage of such an approach is that regardless of the time-varying open area the flow in the perforation holes is constantly choked. It ensures proper operation of the TNC system, because the ventilation intensity is independent of the external flow conditions. Opening and closing of the perforation holes may be achieved by sliding two perforated panels (stacked on top of each other) by a tiny distance, usually equal to the hole diameter (0.1 mm–0.3 mm). This oscillation is able to seal and unblock the holes in a very short time, introducing the requested 1/rev cyclic control. Another approach could be to equip the cavity with a special membrane (diaphragm) that could move vertically, periodically obstructing the perforation holes when supplied with proper pressure.

5. Results of numerical simulations

The main benefits of the TNC method (in terms of noise attenuation) are depicted in Figs. 3 and 4 for steady and unsteady modes of operation, respectively. The reference in-plane acoustic pressure p'/p_0 (p_0 – ambient pressure) fluctuation in time t/T (T – period of rotation), recorded at a near-field location of $1.11R$ (i.e. $1.5c$ off the tip, R – rotor radius), has a typical thickness impulse shape, almost symmetrical and of large negative amplitude (highlighted in black colour in both figures), as described in Section 1. In a steady mode of operation (permanent suction and blowing streams) the resultant signal (highlighted in red colour in Fig. 3) is positively affected by TNC, regardless of the azimuthal position of the observer (no directivity pattern). The peak amplitude of p' is reduced by 45% (the corresponding root mean square of p' is lowered by 31%), while the duration time is slightly extended (mitigating the impulsive nature of the pulse). The effective anti-noise waveform (highlighted in blue colour in Fig. 3), generated by the action of TNC device, is derived by subtraction of the reference and the resultant acoustic signals. It is evident that the explored method delivers

the requested noise cancelling property, characterized by suitable impulse timing, width, and shape, but with too low amplitude. Unfortunately, the accompanying cost of the application of TNC in steady mode is high with respect to the aerodynamic performance (even without taking into account the additional energy required to transport fluid to/from the tip). The penalty in rotor shaft torque is equal to 35%, leaving no feasibility of real-world adoption.
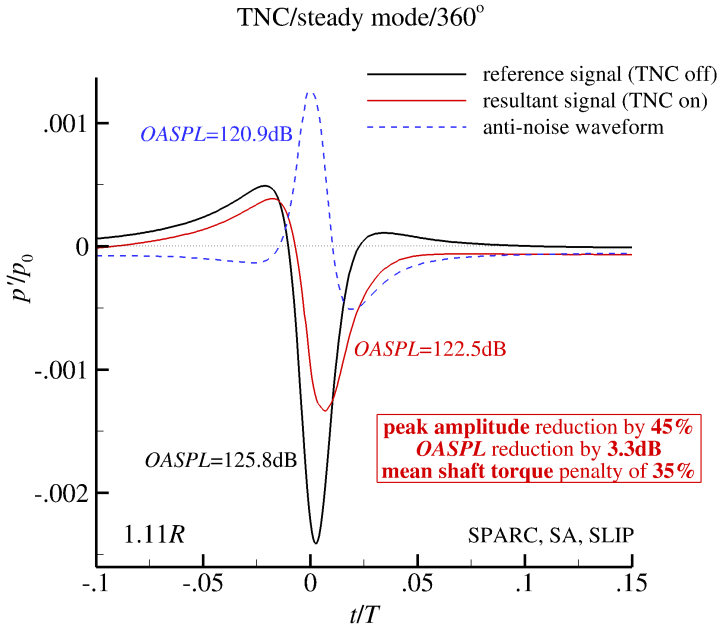
TNC/steady mode/360°

FIG. 3. In-plane acoustic pressure p'/p_0 fluctuation in time t/T recorded at $1.11R$ (TNC in steady mode of operation).

On the contrary, the TNC method in unsteady mode of operation (designed for forward flight conditions) delivers a comparable acoustic pressure signal to a steady approach (shape of the main pulse, Fig. 4) with 4.8 times lower required mass flow rate and 3.1 times lower price (11% in terms of the shaft torque increase). It is accomplished by a proper cyclic limitation (with frequency of 1/rev) of surface ventilation to a specific range of the azimuthal position of the advancing blade. For the analysed case this interval is equivalent to 75° of rotation. The peak amplitude of p' is reduced by 42%, while the corresponding root mean square of p' is lowered by 26%. An important negative implication is introduction of two new acoustic disturbances (of negative and positive signs), radiated exactly at the moments of periodic activation and deactivation of transpiration. It is a direct consequence of a sudden change in time of the type of wall boundary condition (solid vs. permeable surface), not only affecting the resultant thickness

impulse, but also the anti-noise signal waveform. However, it is estimated (based on [32]) that steady centrifugal tip blowing of $0.3\,\mathrm{kg}\cdot\mathrm{s}^{-1}$ at a comparable tip Mach number and blade radius could result in approx. 2% additional rotor torque penalty due to the presence of an internal flow in the duct. Moreover, the experiment proved that the peak mass-flux that can be achieved using sinusoidal (unsteady) 1/rev control constitutes 60% of the initial value. It is necessary to emphasize that it is not the blowing, but the suction system of TNC that constitutes a major challenge for application. Not only the expected suction mass flow rate is 2.4 times higher, but also the centrifugal forces are acting against the flow direction.
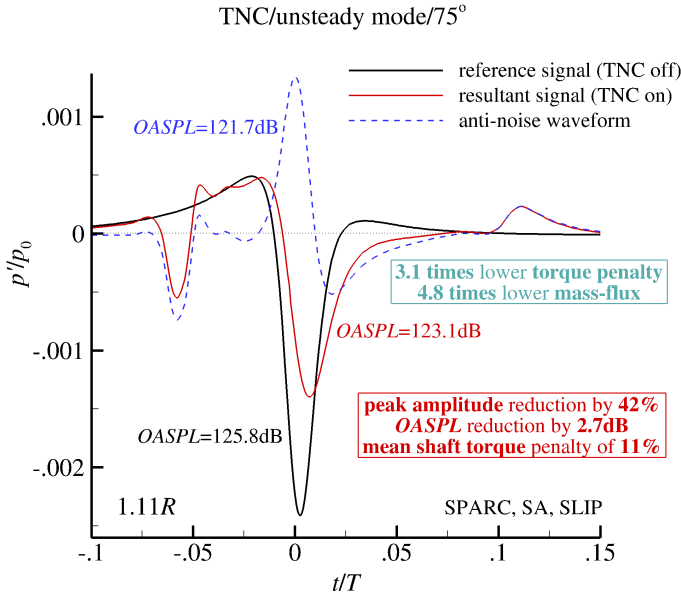

FIG. 4. In-plane acoustic pressure p'/p_0 fluctuation in time t/T recorded at $1.11R$ (TNC in unsteady mode of operation).

A brief comparison of the aerodynamic characteristics of the reference rotor (TNC off) and of the configurations with the TNC device activated (TNC on) permanently (steady mode/360°) or cyclically (unsteady mode/75°) is presented in Table 4. The average rotor thrust c_t and torque c_q, and blade pitching moment c_m coefficients are defined by:

$$(5.1) \qquad c_t = \frac{F_t}{\frac{1}{2}\rho_0 V_T^2 \pi R^2}, \quad c_q = \frac{M_q}{\frac{1}{2}\rho_0 V_T^2 \pi R^3}, \quad c_m = \frac{M_\theta}{\frac{1}{2}\rho_0 V_T^2 \pi R^3}$$

(where $F_t\,[\mathrm{N}]$ – rotor thrust force, $M_q\,[\mathrm{N}\cdot\mathrm{m}]$ – rotor shaft torque, and $M_\theta\,[\mathrm{N}\cdot\mathrm{m}]$ – blade pitching moment). It is clearly noticeable that for the reference configu-

ration (Purcell's model rotor) and selected conditions (hover with the full-scale tip Mach number of 0.661) analysed in the paper, the values of c_t and c_m are low. It is not only because the collective θ is fixed at 1.5°, but also the rigid blades are untwisted and constructed using a symmetrical airfoil (NACA 0012). Indeed, with the TNC system operating constantly (steady transpiration), the average c_t is reduced from $1.1 \cdot 10^{-4}$ to $0.2 \cdot 10^{-4}$ – a significant relative difference that appears mainly due to chosen operating conditions (low-thrust) and simplified rotor blade geometry (i.e. no twist). For the TNC device in an intermittent mode (unsteady transpiration) this disparity is much less severe, resulting in a drop just below 9% (i.e. from $1.1 \cdot 10^{-4}$ to $1.0 \cdot 10^{-4}$). In parallel, the average c_q is augmented by the proposed method of thickness noise control in either state of operation. It is evident that the rotor torque is increased from $2.6 \cdot 10^{-5}$ to $3.5 \cdot 10^{-5}$ (by 35%) or to $2.9 \cdot 10^{-5}$ (by 11%), for the steady and the unsteady approaches to TNC respectively. On the contrary, the blade pitching moment coefficients c_m depicted in Table 4 are not time-averages, but instantaneous values calculated at an exemplary azimuthal position angle $\psi = 0°$. It is apparent that the surface ventilation shifts the chordwise distribution of loads. The reference value of $0.1 \cdot 10^{-7}$ is increased up to $3.4 \cdot 10^{-7}$ (TNC on/steady mode/360°) or $1.5 \cdot 10^{-7}$ (TNC on/unsteady mode/75°), even though at $\psi = 0°$ the transpiration is not active for the latter configuration (enabled between 37.5° and 112.5°). Considering the operation of a full-scale helicopter rotor in a forward flight (equipped with twisted and elastic blades, based on modern non-symmetrical airfoils), it must be stressed out that any modification of the sectional lift, drag or pitching moment characteristics (e.g. introduced by TNC) would necessitate an adaptation of the rotor trimming procedure. This important topic is not covered by the current analysis.

Table 4. Average rotor thrust c_t and torque c_q, and blade pitching moment c_m coefficients.

Case	c_t	c_q	c_m
reference (TNC off)	$1.1 \cdot 10^{-4}$	$2.6 \cdot 10^{-5}$	$0.1 \cdot 10^{-7}$
TNC on/steady mode (360°)	$0.2 \cdot 10^{-4}$	$3.5 \cdot 10^{-5}$	$3.4 \cdot 10^{-7}$
TNC on/unsteady mode (75°)	$1.0 \cdot 10^{-4}$	$2.9 \cdot 10^{-5}$	$1.5 \cdot 10^{-7}$

The overall sound pressure level $OASPL\,(\mathrm{dB})$ acoustic norm is evaluated using formulas:

$$(5.2) \quad OASPL\,(\mathrm{dB}) = 10 \log \frac{p'^2_{\mathrm{rms}}}{p'^2_{\mathrm{ref}}}, \quad p'_{\mathrm{rms}} = \frac{1}{N^2} \sqrt{\sum_{k=1}^{N} p'^2_k} \ \mathrm{Pa}, \quad \mathrm{p}'_{\mathrm{ref}} = 20\,\mu\mathrm{Pa},$$

where: p'_{rms} – root mean square of p', p'_{ref} – threshold of human hearing, N –

sample count, and p'_k – successive acoustic pressure values in time. A single blade passage (half the period of rotation T) is probed and analysed with a temporal resolution of 1440 time steps of the numerical scheme per period T, i.e. $N = 720$. For an in-plane observer positioned at $1.11R$ the impact of the TNC technique on the reduction of the overall sound pressure level $OASPL$ is comparable for steady and unsteady modes of operation, reaching $3.3\,\text{dB}$ and $2.7\,\text{dB}$, respectively. It is worth to remind that a drop of $OASPL$ by $6\,\text{dB}$ signifies two times lower p'_{rms}. Additionally, the acoustic pressure p' signals of Figs. 3 and 4 are transformed into the frequency domain by employing the Discrete Fast Fourier Transform (DFFT). The resulting sound pressure level SPL (dB) spectra of Fig. 5 indicate that for the first 20 rotor harmonics n (the most important from the point of view of detection and annoyance) the achievable gains in a steady mode (TNC on/360°) are ranging from $3.0\,\text{dB}$ to $8.5\,\text{dB}$. In an unsteady operation (TNC on/75°) the action of TNC reveals a more complex behaviour. For some rotor harmonics (i.e. 2nd, 7th, and 16th) the SPL is only slightly damped, while for others it is more significantly suppressed, in case of the 1st, 5th, 12th, and 20th even surpassing the efficiency of the permanently present surface transpiration. Probably, the wavy character of the envelope displayed in Fig. 5 is caused by the appearance of secondary peaks in the signal, recorded in the time domain due to sudden activation and deactivation of ventilation (Fig. 4). Unfortunately, this uneven effectiveness pattern is reflected in an increased $OASPL$ value by $0.6\,\text{dB}$ compared to the steady control case.
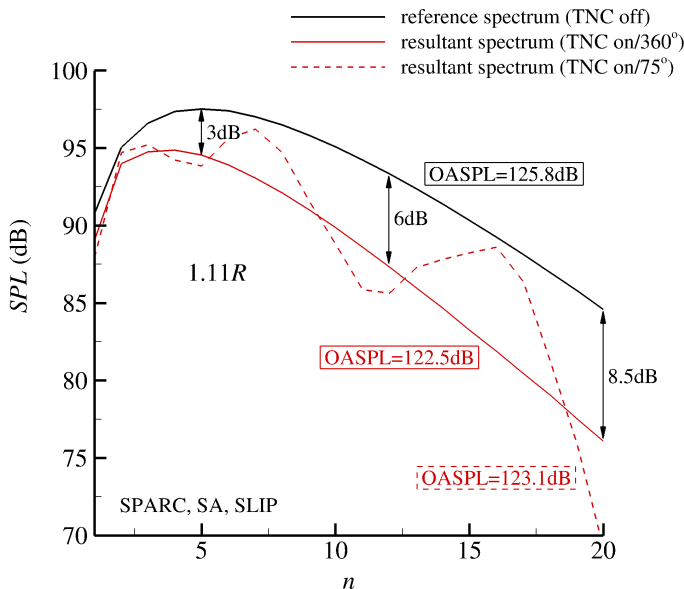

FIG. 5. Sound pressure level spectrum SPL (dB).

An important aspect of any new rotor noise control system designed for forward flight conditions is its efficiency at off-target positions (directivity). Apart from probing the acoustic pressure signal at the target location p_0 (centre), four additional points are investigated: p_1 (left), p_2 (right), p_3 (bottom), and p_4 (top) – see Table 5 and Fig. 6. The data recorded at the point p_0 has already been analysed in Figs. 3, 4 and 5 for all three configurations (i.e. reference and with TNC in steady and unsteady modes of operation). The quarter-chord line of the blade at 90° of azimuth (rotating in clock-wise direction) is positioned on the z-axis. The x-axis is starting at the leading edge and pointing downstream, along the chord, while the y-axis is starting at the rotor plane and pointing upwards. In such a reference system the point p_0 (centre) is placed at a radial station of $1.11R$ and x-, y-, and z-coordinates of $(0.25c, 0.0c, 15.22c)$ – black colour in Fig. 6. When a line connecting the quarter-chord point at the tip (highlighted

Table 5. **Location of acoustic pressure p' probing points $p_0 - p_4$ in space.**

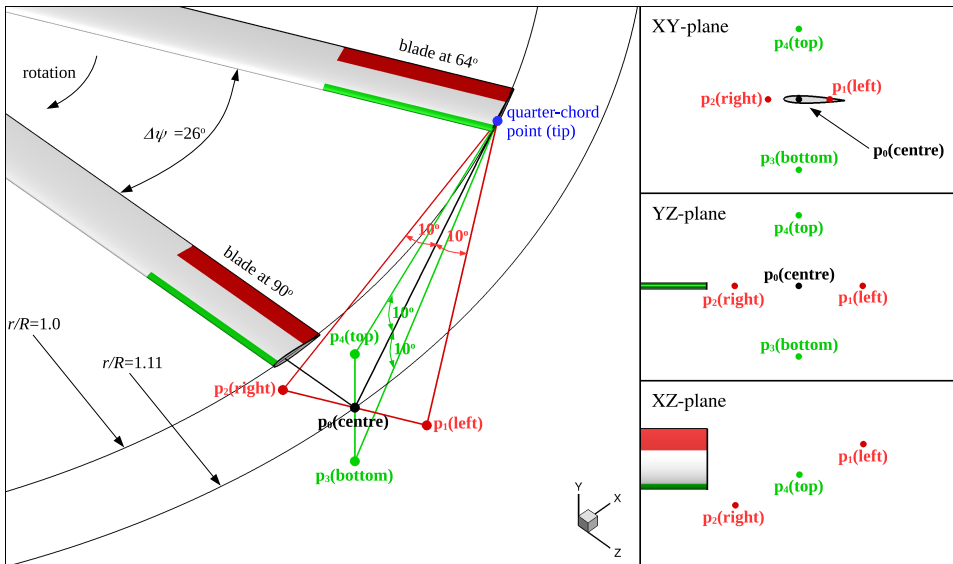| Designation	x	y	z	Radial position	Description
p_0 (centre)	$0.25c$	$0.0c$	$15.22c$	$1.11R$	reference (target)
p_1 (left)	$0.76c$	$0.0c$	$16.27c$	$1.19R$	$10°$ to the left of p_0
p_2 (right)	$-0.26c$	$0.0c$	$14.17c$	$1.03R$	$10°$ to the right of p_0
p_3 (bottom)	$0.25c$	$-1.16c$	$15.22c$	$1.11R$	$10°$ below p_0
p_4 (top)	$0.25c$	$1.16c$	$15.22c$	$1.11R$	$10°$ above p_0

FIG. 6. Location of acoustic pressure p' probing points p_0–p_4 in space.

in blue colour) with the target observer location is at right angle, a maximum emission of thickness noise is to be expected. For the baseline point p_0 it corresponds to approx. 26° earlier azimuthal position of the blade ψ (i.e. to $\psi = 64°$). Points p_1 (left) and p_2 (right) are placed 10° to the left and 10° to the right of the maximum radiation line, at radial stations of $1.19R$ ($0.76c$, $0.0c$, $16.27c$) and $1.03R$ ($-0.26c$, $0.0c$, $14.17c$), respectively – red colour in Fig. 6. The remaining points p_3 (bottom) and p_4 (top) are positioned 10° below and 10° above the rotor plane, at $1.11R$, i.e. at x-, y- and z-coordinates of ($0.25c$, $-1.16c$, $15.22c$) and ($0.25c$, $1.16c$, $15.22c$) accordingly – green colour in Fig. 6. The choice of the deviation angle of 10° (instead of e.g. 15°) is dictated by a very close proximity of the point p_0 (centre) to the tip of the blade and a desire to keep the same value for all investigated off-target locations: p_1, p_2, p_3 and p_4. Any higher deviation angle would shift the point p_2 (right) into the rotor disc, therefore making the p' extraction procedure impossible.

In theory, a constant transpiration mass-flow rate of the steady mode of TNC ensures generation of a fixed anti-noise signal shape, regardless of the azimuthal position of the observer (perfect horizontal directivity pattern). For each of the analysed locations: p_0 (centre), p_1 (left) and p_2 (right) the negative peak amplitude of thickness noise reduction is practically the same for both variants of the method (within 3% margin). It suggests no variability in the left/right directivity for 10° spreading of the acoustic pulse from the source. Such a feature of the directionality seems to be attractive from the point of view of potential application in forward flight, but still higher angles than 10° should be investigated to confirm the exact borders of the maximum efficiency zone. On the other hand, two new acoustic disturbances, introduced by intermittent activation and deactivation of the surface ventilation (TNC in unsteady mode), play a significant role depending on the radial placement of the observer. In contrast to thickness noise (i.e. constant sources and sinks of mass, rotating in space), this radiation is caused by a sudden increase of suction and blowing mass-fluxes from 0 to maximum value in a very short time (i.e. unsteady sources and sinks of mass, rotating in space). The resulting negative and positive impulses are associated with blade azimuthal positions ψ of 37.5° and 112.5°, therefore released at earlier or later times compared to the maximum of thickness noise radiation for points: p_0, p_1, and p_2 – see Fig. 7. The amplitude and the arrival time of these disturbances only slightly vary, in accordance to the distance (between the acoustic source and the extraction points at emission time) and the amplification by the Doppler effect. Due to large differences in the azimuthal position of the maximum radiation for points: p_0, p_1, and p_2, the main thickness pulse amplitude is highly dependent on the radial location ($1.5c$, $2.6c$ and $0.4c$ off the blade tip respectively). As a consequence, the relative importance of the acoustic repercussions of the switching on/off phase is growing, while moving away

from the rotor. As a result, the efficiency of the TNC method, in terms of the overall sound pressure level reduction ($\Delta OASPL$), is dependent on the distance, greatly varying for points: p_0 (2.7 dB), p_1 (0.5 dB), and p_2 (5.2 dB). It implies that the instantaneous cyclic activation and deactivation of surface transpiration may be further improved by a certain transient period that could smooth out the introduced disturbances, leaving the total noise attenuation less affected.
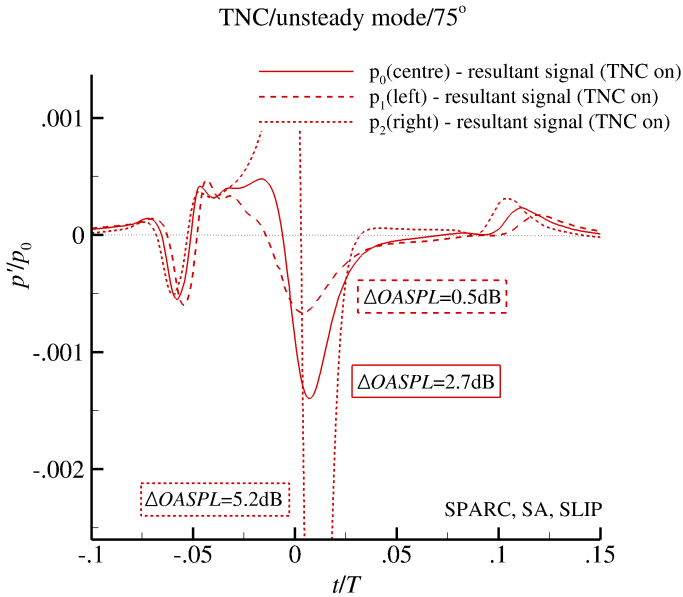

FIG. 7. In-plane acoustic pressure p'/p_0 fluctuation in time t/T recorded at points p_0–p_2 (TNC in unsteady mode of operation).

For each of the investigated locations: p_0 (centre), p_3 (bottom) and p_4 (top) the negative peak amplitude of thickness noise reduction is again nearly the same for both variants of the TNC method (within 3% margin). It reveals no variability in the up/down directivity pattern for 10° vertical spreading of the acoustic impulse from the source, but higher angles than 10° should be analysed to verify the precise boundaries of the maximum efficiency range. The acoustic disturbances introduced by action of the abrupt activation of the transpiration play a less significant role here, but still the efficiency of the TNC method (in unsteady mode), in terms of the overall sound pressure level reduction, is noticeably affected for points: p_0 (2.7 dB), p_3 (1.6 dB), and p_4 (2.3 dB). It confirms that the applied instantaneous cyclic control of ventilation could benefit from a smoother transition.

It is necessary to emphasize that for numerical reasons mentioned in Section 3, the quoted acoustic pressure pulses have been inspected at locations p_0–p_4, positioned in very close proximity of the blades. In principle, the far-field

noise characteristics and the radiation directivity pattern are difficult to assess based on such limited near-field information. The introduced signals are analysed at a distance shorter than the extent of the source and the expected wavelengths of low-frequency contents of the associated spectra. Moreover, the probes are placed in regions where a substantial tip flow influence is still present that may not propagate to the far-field. On the other hand, so near-field acoustic data is rarely published for helicopter rotors operating in hover conditions. Therefore, both the rotor geometry and the reference observer location (p_0) chosen for quantification of the impact of the TNC method have been established according to the sole available experimental study of Purcell who compared sounds recorded at $1.11R$ and $3.0R$ [31]. For the tip Mach number of 0.9 (thickness, loading and high-speed impulsive noise emission), the basic shapes of the in-plane pulses investigated in the near- and far-field were similar. With the exception of the obvious amplitude difference due to the increased distance, the long range signal seemed to be only slightly more symmetric. Hence, the close-range data may be valuable at the initial stage of the research, keeping in mind that this information is inherently included in the CFD simulation results and merely requires additional acoustic post-processing. Furthermore, because the main mechanism of TNC is almost identical to pure thickness noise generation (as described in Section 2), the near-field data may be useful in the preliminary assessment of the proposed method. The presented comparative evaluation of two rotor systems (reference and equipped with TNC), expressed in terms of the overall sound pressure level $OASPL$ (dB) reduction, should be less affected by near-field placement of the microphones, since it contains the same near-field background, regardless of the configuration. However, such statements remain to be verified by a proper acoustic analogy study of the TNC by surface ventilation.

6. Conclusions

The paper describes in detail the development of the TNC (Thickness Noise Control) method, designed for in-plane helicopter rotor harmonic noise reduction in forward flight. It is based on incorporation of multiple cavities at the blade tip (covered by perforated panels) and connected to low and high pressure supplies. Intensive suction and blowing of air, distributed symmetrically at the front and rear portions of the chord, allow for generation of the anti-noise impulse which, if added to the reference signal, results in significant attenuation of the sound radiation. The results of numerical simulations (SPARC solver with SA turbulence and BD transpiration models), obtained for the UH-1H model rotor of Purcell operating in low-thrust hover conditions, suggest that the near-field acoustic pressure p' fluctuations may be effectively lessened by action of TNC. The peak amplitude of p' is reduced by 45% (in steady mode) or 42% (in un-

steady mode), while the overall sound pressure level $OASPL$ is limited by 3.3 dB or 2.7 dB respectively. Moreover, the most important low-frequency bands (i.e. first 20 rotor harmonics) are characterized by substantial damping of sound pressure level SPL, in the range of 3.0 dB–8.5 dB (steady mode) or 0.5 dB–15.5 dB (unsteady mode). The periodic activation of TNC in a cyclic manner, intended for forward flight state, efficiently brings down the shaft torque penalty to 11%, compared to the initially very high value of 35%. It is a direct consequence of the restriction of blade surface transpiration to approx. $1/5^{\text{th}}$ of the rotor revolution, reducing not only the introduced flow losses (3.1 times), but also the required ventilation mass flux (4.8 times). The investigated TNC method in the proposed new (time-dependent) schedule of operation provides a desired noise cancelling property and appears to constitute a practicable remedy to helicopter rotor harmonic noise emission of future designs. However, it is important to emphasize that the activation/deactivation of the transpiration streams of TNC introduces undesirable acoustic side-effects. Two pressure disturbances of opposite amplitudes are emitted and added to the noise signature. Fortunately, due to their different arrival times, the efficiency of the attenuation of the main pressure pulse amplitude is not affected. Still, a more gradual operation is recommended for future studies. In practice, air supply and exhaust valves are not able to operate instantly, therefore the introduced disturbances should be smoothed out significantly. To avoid confusion, it is important to underline that the presented TNC method is active in terms of flow control strategy used (surface suction and blowing), but passive in nature from the point of view of acoustic attenuation. It does not rely on any sort of sensors or feedback mechanisms whatsoever, so the presented method should not be considered as an Active Noise Control (ANC) strategy. The thickness noise source is purely kinematic and dependent on the blade shape and movement only which are known a priori.

The presented numerical results are very promising in terms of potential application of the TNC system to the reduction of acoustic radiation, but are also far from being complete. The remaining key questions are: what is the impact of the investigated method on the detailed directivity pattern of sound emission from the advancing blade, and moreover, what is the effect of TNC regarding the out-of-plane locations, and how other sources of the aerodynamic noise, such as the dipole (loading) and the quadrupole components, are affected? Some improvements in a peak amplitude of the anti-noise impulse (hence, the achievable levels of attenuation), and in associated drag penalty, are still feasible. As the next step two options will be explored first. So far, only a uniform transpiration velocity V_{t} (and mass flux) has been applied for each of the perforated plates. It is possible to easily adapt the local intensity of V_{t} to the normal velocity values V_{n} (known a priori) present at the ventilated surface – a major contributor to the acoustic potential of the thickness term of Eq. (1.1). In principle it is permissible

to vary the number of perforated panels used, their dimensions and chordwise or spanwise arrangement at the blade tip. Additionally, the hole number and size (i.e. diameter and length), as well as the distribution over the permeable surface (uniform or space varying) have to be chosen. The implemented perforated wall boundary condition (based on the empirical BD transpiration model) allows to set the aerodynamic (effective) porosity factor (constant or variable) and the outflow angle (straight hole axis inclination) only. Therefore, the local (continuous) distribution of the transpiration mass-flux is imposed, instead of the discrete perforation holes properties. Until now only uniform porosity panels have been tested, but the non-uniform approach could lead to improved cancellation of the main source of thickness noise (i.e. wall normal velocity). Such spatial adaptation of p_{aero} to the magnitude of V_{n} (due to blade motion) would necessitate the aerodynamic porosity to have maxima near the leading (forward cavity) and trailing (rearward cavity) edges of the rotor blade tip, not only increasing the efficiency of TNC, but also limiting the required mass flow rate of suction and blowing streams. It is worth noting that it is the time derivative of the monopole integral of Eq. (1.1) that is responsible for sound radiation, not the value itself. This provides another opportunity to accommodate unsteady suction and blowing rates in order to reach better efficiency of TNC. Fortunately, the built-in fast-switching air supply and exhaust valves would not only allow for time-varying opening and closing, but also for a convenient deactivation of the system in flight conditions when its operation is not required, lowering the related performance penalty. The study will be continued using the CFD methodology (i.e. SPARC solver), applicable mainly to aerodynamic loading predictions, and supplemented by a recently developed rotor acoustic code [33], based on Ffowcs Williams–Hawkings analogy (Farassat's formulation 1A) [2, 3] and capable of modelling noise generation mechanisms (sources) and propagation appropriately. Further investigations are necessary to confirm whether the near-field noise reductions obtained with TNC really extend to the far-field.

Acknowledgments

References

1. F.H. Schmitz, *The challenges and possibilities of a truly quiet helicopter*, Journal of the American Helicopter Society, **61**, 4, 041001, 1–33, 2016.

2. F. Farassat, *Derivation of formulations 1 and 1A of Farassat*, NASA Langley Technical Memorandum, TM-2007-214853, 1–20, 2007.

3. J.E. Ffowcs Williams, D.L. Hawkings, *Sound generation by turbulence and surfaces in arbitrary motion*, Philosophical Transactions of the Royal Society of London, **264**, 1151, 321–342, 1969.

4. F.H. Schmitz, *Rotor noise*, Aeroacoustics of Flight Vehicles: Theory and Practice; Volume 1: Noise Sources, H.H. Hubbard [ed.], NASA Langley Reference Publication 1258, United States, 65–149, 1991.

5. K.S. Brentner, F. Farassat, *Modeling aerodynamically generated sound of helicopter rotors*, Progress in Aerospace Sciences, **39**, 2–3, 83–120, 2003.

6. W.R. Splettstoesser, B. van der Wall, B. Junker, K.J. Schultz, P. Beaumier, Y. Delrieux, P. Leconte, P. Crozier, *The ERATO programme: wind tunnel test results and proof of design for an aeroacoustically optimised rotor*, Proceedings of the 25th European Rotorcraft Forum, Rome, B7, 1–15, 1999.

7. M. Mosher, *Acoustic measurements of a full-scale rotor with four tip shapes, Vol. 1*, NASA Ames Technical Memorandum, NASA-TM-85878-VOL-1, 1–89, 1984.

8. M. Mosher, *Acoustic measurements of a full-scale rotor with four tip shapes, Vol. 2*, NASA Ames Technical Memorandum, NASA-TM-85878-VOL-2, 1–348, 1984.

9. F.H. Schmitz, D.A. Boxwell, R. Vause, *Acoustically swept rotor*, United States Patent, 4168939, 1–23, 1979.

10. B. Edwards, *Psychoacoustic testing of modulated blade spacing for main rotors*, NASA Langley Contractor Report, NASA/CR-2002-211651, 1–50, 2002.

11. B. Hagerty, S. Kottapalli, *Boeing SMART rotor full-scale wind tunnel test data report*, NASA Ames Technical Memorandum, NASA/TM-2012-216048, 1–20, 2012.

12. B.W. Sim, R.D. Janakiram, B.H. Lau, *Reduced in-plane, low-frequency noise of an active flap rotor*, Journal of the American Helicopter Society, **59**, 2, 022002, 1–17, 2014.

13. T.R. Norman, C. Theodore, P. Shinoda, D. Fuerst, U.T.P. Arnold, S. Makinen, P. Lorber, J. O'Neill, *Full-scale wind tunnel test of a UH-60 individual blade control system for performance improvement and vibration, loads, and noise control*, Proceedings of the American Helicopter Society 65th Annual Forum, Grapevine, 1–20, 2009.

14. Ch. Kessler, *Active rotor control for helicopters: motivation and survey on higher harmonic control*, CEAS Aeronautical Journal, **1**, 3, 3–22, 2011.

15. E.R. Booth, M.L. Wilbur, *Acoustic aspects of active-twist rotor control*, Journal of the American Helicopter Society, **49**, 1, 3–10, 2004.

16. C.D. Sargent, F.H. Schmitz, *Fundamental experimental studies supporting on-blade tip air blowing control of in-plane rotor harmonic noise*, Proceedings of the AIAA 33rd Aeroacoustics Conference, Colorado Springs, 2012-2140, 1–20, 2012.

17. Y. Shi, T. Li, X. He, L. Dong, G. Xu, *Helicopter rotor thickness noise control using unsteady force excitation*, Applied Sciences, **9**, 7, 1351, 1–17, 2019.

18. O. Szulc, P. Doerffer, *Numerical study of potential application of active suction and blowing through blade tip perforation to reduction of helicopter rotor thickness noise*, Journal of Physics: Conference Series, **1101**, 012042, 1–6, 2018.

19. P.P. Doerffer, R. Bohning, *Modelling of perforated plate aerodynamics performance*, Aerospace Science and Technology, **4**, 8, 525–534, 2000.

20. S. Platzer, J. Rauleder, M. Hajek, J. Milluzzo, *Experimental and computational investigation on rotor blades with spanwise blowing*, Proceedings of the 42nd European Rotorcraft Forum, Lille, 1–15, 2016.

21. T. Young, B. Mahony, B. Humphreys, E. Totland, A. McClafferty, J. Corish, *Durability of hybrid laminar flow control (HLFC) surfaces*, Aerospace Science and Technology, **7**, 181–190, 2003.

22. F. Magagnato, *KAPPA – Karlsruhe parallel program for aerodynamics*, TASK Quarterly, **2**, 2, 215–270, 1998.

23. P.R. Spalart, S.R. Allmaras, *A one-equation turbulence model for aerodynamic flows*, Proceedings of the AIAA 30th Aerospace Sciences Meeting and Exhibit, Reno, 92-0439, 1–22, 1992.

24. P. Doerffer, O. Szulc, *Shock wave smearing by wall perforation*, Archives of Mechanics, **58**, 6, 543–573, 2006.

25. P. Doerffer, O. Szulc, *Application of the passive control of shock wave to the reduction of high-speed impulsive noise*, International Journal of Engineering Systems Modelling and Simulation, **3**, 1–2, 64–73, 2011.

26. O. Szulc, P. Doerffer, P. Flaszynski, T. Suresh, *Numerical modelling of shock wave-boundary layer interaction control by passive wall ventilation*, Computers & Fluids, **200**, 104435, 1–21, 2020.

27. O. Szulc, P. Doerffer, F. Tejero, *Passive control of rotorcraft high-speed impulsive noise*, Journal of Physics: Conference Series, **760**, 012031, 1–9, 2016.

28. P. Doerffer, O. Szulc, *Numerical simulation of model helicopter rotor in hover*, TASK Quarterly, **12**, 3, 227–236, 2008.

29. O. Szulc, Passive control of shock wave-boundary layer interaction, PhD Dissertation, Institute of Fluid-Flow Machinery, Poland, 1–248, 2019, DOI:10.13140/RG.2.2.29478.06721 [in Polish].

30. P. Doerffer, O. Szulc, *Aerodynamic and aero-acoustic analysis of helicopter rotor blades in hover*, eScience on Distributed Computing Infrastructure; Achievements of PLGrid Plus Domain-Specific Services and Tools, M. Bubak, J. Kitowski, K. Wiatr [eds.], Springer, Switzerland, 429–444, 2014.

31. T.W. Purcell, *CFD and transonic helicopter sound*, Proceedings of the 14th European Rotorcraft Forum, Milano, 2, 1–17, 1988.

32. A. Karpatne, J. Sirohi, B.Y. Min, D. Shannon, *Experimental and numerical study of internal flow through a rotating duct*, Journal of the American Helicopter Society, **62**, 032010, 1–12, 2017.

33. T. Suresh, O. Szulc, P. Flaszynski, P. Doerffer, *Prediction of helicopter rotor noise in hover using FW-H analogy*, Journal of Physics: Conference Series, **1101**, 012041, 1–8, 2018.